

Quantum electrodynamic corrections for molecules: Vacuum polarisation and electron self energy in a two-component relativistic framework*

Kjell Janke,¹ Andrés Emilio Wedenig,¹ Peter Schwerdtfeger,^{2,3} Konstantin Gaul,¹ and Robert Berger¹

¹*Fachbereich Chemie, Philipps-Universität Marburg,
Hans-Meerwein-Straße 4, 35032 Marburg, Germany*

²*Centre for Theoretical Chemistry and Physics, The New Zealand Institute for Advanced Study (NZIAS),
Massey University Albany, Private Bag 102904, Auckland 0745, New Zealand*

³*Laboratoire Kastler Brossel, Sorbonne Université, CNRS,
ENS-PSL Research University, Collège de France*

(Dated: November 14, 2024)

Vacuum polarisation (VP) and electron self energy (SE) are implemented and evaluated as quantum electrodynamic (QED) corrections in a (quasi-relativistic) two-component zeroth order regular approximation (ZORA) framework. For VP, the Uehling potential is considered, and for SE, the effective potentials proposed by Flambaum and Ginges as well as the one proposed by Pyykkö and Zhao. QED contributions to ionisation energies of various atoms and group 2 monofluorides, group 1 and 11 valence orbital energies, ${}^2P_{1/2} \leftarrow {}^2S_{1/2}$ and ${}^2P_{3/2} \leftarrow {}^2S_{1/2}$ transition energies of Li-, Na-, and Cu-like ions of nuclear charge $Z = 10, 20, \dots, 90$ as well as $\Pi_{1/2} \leftarrow \Sigma_{1/2}$ and $\Pi_{3/2} \leftarrow \Sigma_{1/2}$ transition energies of BaF and RaF are presented. Furthermore, perturbative and self-consistent treatments of QED corrections are compared for Kohn-Sham orbital energies of gold. It is demonstrated, that QED corrections can be obtained in a two-component ZORA framework efficiently and in excellent agreement with corresponding four-component results.

I. INTRODUCTION

Relativistic effects play a crucial role for the quantitative description of heavy-element containing molecules [1, 2]. The usual starting point for a relativistic description of the electronic motion in a molecule is the free-particle Dirac equation [3, 4] combined with a classical Coulomb-type potential for the description of leading order particle-particle interactions [5]. This formalism describes the motion of electrons in accord with special relativity, but not its interactions, which are due to the Coulomb potential instantaneous. Within quantum electrodynamics (QED), i.e. the relativistic theory of the electromagnetic force, interactions are not instantaneous but are mediated by virtual photons at the speed of light. Therefore, the Coulomb potential arises only as leading order contribution to the electromagnetic particle-particle interaction in a perturbation theory expansion in the fine-structure constant. Largest QED effects are expected for the electron-nucleus potential [6], to which we will refer in the following exclusively and as retardation effects of the electron-electron interactions. The latter are however usually not as important as QED corrections of the electron-nucleus potential. Larger corrections to the electron-electron interactions are expected via the Breit interaction [7], which appears due to consideration of current-current interactions and the inclusion of the correct gauge of the interaction within a Lorentz invariant framework. Photon-frequency dependent retardation corrections to the Breit interaction are usually less

important than QED corrections of the electron-nucleus potential considered in this work. It is expected that QED corrections reduce the total relativistic effects by about 1 % in heavy atom containing-molecules [8, 9]. For the hydrogen atom this QED correction of the electron-nucleus potential leads to the so-called Lamb shift, which splits $ns_{1/2}$ and $np_{1/2}$ states in one-electron systems [10]. In the search for new physics beyond the standard model, high-precision spectroscopy is an essential tool to test the fundamental symmetries, such as space- and time-reversal parity and its violations [11, 12]. Because of the numerically small effects, it is important to investigate systems with a number of traits, which enhance effects of these violations. Certain molecules are particularly suited for such purposes. One promising candidate is radium monofluoride (RaF). It was first proposed because of its predicted nuclear-spin-dependent parity violation and expected suitability for laser cooling [13, 14]. The pear-shaped octupole deformation [15, 16] of the heavy ${}^{222,224,226}\text{Ra}$ isotopes enhances symmetry violation effects further. Synthesis of the open-shell short-lived isotopically pure radioactive RaF molecules and successive spectroscopy was first achieved with the collinear resonance ionisation spectroscopy (CRIS) method at the ISOLDE ion-beam facility at CERN [17]. Applicable for other molecules, such as RaOH, RaO, RaH, AcF and ThO, and nuclei with half-lives of just milliseconds, it paved the way for high-precision spectroscopy of radioactive isotope containing molecules. In recent experiments, the rovibronic structure of ${}^{226}\text{Ra}^{19}\text{F}$ was obtained with a resolution, which is two orders of magnitude larger compared to previous experiments [18]. Also, eleven electronic states and excitations were reported [19]. Thus, theoretical predictions and proposals of suited molecules for precision tests play an essential role. However, as the

* Parts of this work were reported in preliminary form in K. Janke, M.Sc. thesis, Philipps-Universität Marburg, 2023, and in A. E. Wedenig, B.Sc. thesis, Philipps-Universität Marburg, 2022.

experiments have reached unprecedented accuracies, and the investigated symmetry violations are even smaller, it is necessary to develop sophisticated theoretical frameworks further as well. While QED corrections have been studied in atoms for a long time [20–34], they have gained attention in molecular frameworks only recently [35–42]. In high-precision calculations of atoms, the leading order QED corrections have shown to be the missing contributions to the first ionisation energy and electron affinity of the gold atom in order to reach meV accuracy, compared to the experimental values [43]. Pařtka *et al.* also noted, that higher excitations in the coupled cluster (CC) method have less impact on the result, compared to the QED corrections. Because QED contributions grow with increasing nuclear charge, as they are relativistic effects, they are expected to contribute mainly to molecules containing heavy nuclei such as RaF. Overall, the effects in molecules and the influence on properties are largely unknown and it is thus desirable to have efficient, yet accurate, options to approximate the corrections reliably. In this work, the leading order QED corrections are included as effective potentials within the two-component ZORA framework. Within this framework, one can obtain accurate results for the QED corrections, although the overall error of ZORA, compared to four-component approaches, is in the same order of magnitude. This incremental approach allows for an efficient treatment of QED effects in atoms and molecules, suited to predict size, trends and relevance. Results of variational and perturbative treatments are compared to four-component variational and numerical Dirac-Hartree-Fock (DHF) calculations.

II. THEORY

A. Vacuum polarisation

Considering instantaneous electron-positron pair creation and annihilation in vacuum, one obtains a temporary polarisation of the vacuum, which averages out when one considers integration over time. Here, the vacuum polarisation is treated as a perturbation to the electron-nucleus attraction term. The schematic process is shown in Figure 1a, while 1b shows the Uehling process, which assumes the created pair to be free particles.

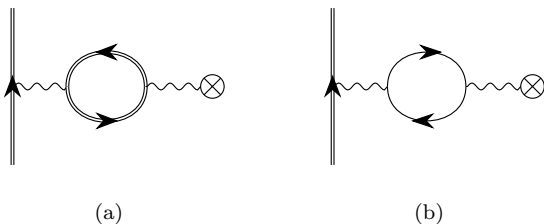


FIG. 1: Feynman diagrams of the exact bound-state VP (a) and Uehling potential (b).

The Uehling potential [44] for the interaction between an electron and point-like nucleus with charge number Z is

$$V_u(\vec{r}) = -\frac{2\alpha}{3\pi} e\phi(\vec{r}) \int_1^\infty \frac{\sqrt{t^2-1}}{t^2} \left(1 + \frac{1}{2t^2}\right) e^{-\frac{2t|\vec{r}|}{\lambda}} dt \quad (1)$$

where α is the fine-structure constant, $\phi(\vec{r}) = \frac{Z}{4\pi\epsilon_0|\vec{r}|}$ is the Coulombic nuclear electrostatic potential with electric constant ϵ_0 , $\lambda = \frac{\hbar}{m_e c} = \alpha a_0$ is the reduced Compton wavelength of the electron, r is the distance between electron and nucleus, a_0 is the Bohr radius, \hbar the reduced Planck constant, e the elementary charge and m_e the electron mass. The integral can be reformulated in terms of modified Bessel functions [45] to obtain an analytical expression. Herein, however, the potential is evaluated using the method by Fullerton and Rinker [46]. Higher order corrections for the vacuum polarisation, such as the Wichmann-Kroll [47] or the Källén-Sabry [48] potentials are not included in this work, since the Uehling potential is by far the largest contribution.

B. Self energy

Other than the VP, the electron self energy is not easily written as a local potential. The fundamental process is the exchange of a virtual photon of an electron with itself at a later point in time. Figure 2 shows the two main processes, which contribute to the correction. The electron is assumed to be a free particle, for the time between emission and absorption.

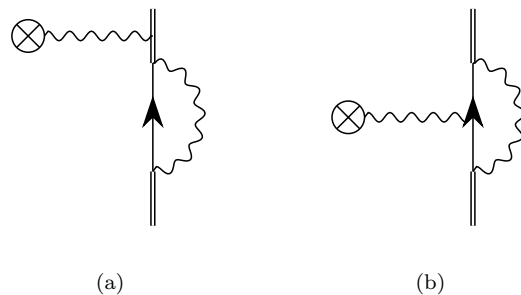


FIG. 2: Self energy (a) and vertex correction (b) of order $\alpha(Z\alpha)$

Herein, the effective potentials, proposed by Flambaum and Ginges [49], as well as the one proposed by Pyykkö and Zhao [50], are considered. The Pyykkö–Zhao potential is an exponential function with two fitting functions, $B_{pz}(Z)$ and $\beta(Z)$, depending on the nuclear charge Z ,

$$V_{pz}(\vec{r}) = B_{pz}(Z) e^{-\beta(Z)|\vec{r}|^2} \quad (2)$$

$$\begin{aligned} B_{pz}(Z)/E_h &= -48.6116 + 1.53666Z + 0.0301129Z^2 \\ \beta(Z)/a_0^{-2} &= -12751.3 + 916.038Z + 5.7797Z^2, \end{aligned}$$

with E_h being the Hartree energy. The fitting functions $B_{pz}(Z)$ and $\beta(Z)$ were obtained from 2s energy shifts of H-like systems with a finite nucleus [51, 52] and 2s M1 hyperfine splittings of H-like systems [53] and Li-like 2s states [54]. The H-like and Li-like reference data were combined and yielded the potential, which can be used for ns energy levels and M1 hyperfine shifts of all elements $Z \geq 29$. The lower nuclear charges were not covered due to the reference data. The Flambaum–Ginges potential was derived more rigorously [49, 55] and splits into three contributions. Connected to the magnetic form factor is a potential, to which we refer as the magnetic contribution V_m . From the electric form factor there arise two potentials, which we denote as the high- and low-frequency contributions, V_h and V_l . The magnetic contribution for a point-like nucleus reads

$$\begin{aligned}
V_m(\vec{r}) &= -e \frac{\alpha\lambda}{4\pi} i\vec{\gamma} \cdot \vec{\nabla} \left[\phi(\vec{r}) \left(\int_1^\infty \frac{e^{-\frac{2t|\vec{r}|}{\lambda}}}{t^2\sqrt{t^2-1}} dt - 1 \right) \right] \\
&= -e \frac{\alpha\lambda}{4\pi} i\vec{\gamma} \cdot \left[\left(\vec{\nabla}\phi(\vec{r}) \right) \left(\int_1^\infty \frac{e^{-\frac{2t|\vec{r}|}{\lambda}}}{t^2\sqrt{t^2-1}} dt - 1 \right) \right. \\
&\quad \left. - \phi(\vec{r}) \frac{2\vec{r}}{\lambda r} \int_1^\infty \frac{e^{-\frac{2t|\vec{r}|}{\lambda}}}{t\sqrt{t^2-1}} dt \right] \\
&= e\phi(\vec{r}) \frac{\alpha\lambda}{4\pi} i\vec{\gamma} \cdot \frac{\vec{r}}{r^2} \left[\int_1^\infty \frac{e^{-\frac{2t|\vec{r}|}{\lambda}}}{t^2\sqrt{t^2-1}} dt - 1 \right. \\
&\quad \left. + \frac{2r}{\lambda} \int_1^\infty \frac{e^{-\frac{2t|\vec{r}|}{\lambda}}}{t\sqrt{t^2-1}} dt \right]
\end{aligned} \tag{3}$$

Only for a point like nucleus, $-\frac{\vec{r}}{r^2}\phi(\vec{r}) = \nabla\phi(\vec{r})$. Compared to the Uehling potential, the magnetic potential does not just include an integral, for which no analytical solution is available, but also the differential operator acting on the product of the integral and the nuclear potential. However, this contribution only shows a dependence on the nuclear charge in terms of the nuclear model. Here, the second equation of 3 was implemented. In comparison, the high frequency contribution reads

$$\begin{aligned}
V_h(\vec{r}) &= A(Z, r) \frac{\alpha}{\pi} e\phi(\vec{r}) \int_1^\infty \frac{e^{-\frac{2t|\vec{r}|}{\lambda}}}{\sqrt{t^2-1}} \left[\left(1 - \frac{1}{2t^2} \right) \right. \\
&\quad \left. \times \left(\ln(t^2-1) + 4 \ln \left(\frac{1}{Z\alpha} + \frac{1}{2} \right) \right) + \frac{1}{t^2} - \frac{3}{2} \right] dt
\end{aligned} \tag{4}$$

In equation (4), Flambaum and Ginges included the cut-off function $A(Z, r)$, with

$$\begin{aligned}
A(Z, r) &= \Theta(Z, \vec{r}) (1.071 - 1.976a^2 \\
&\quad - 2.128a^3 + 0.169a^4) \\
\Theta(Z, r) &= \frac{|\vec{r}|}{|\vec{r}| + 0.07(Z\alpha)^2\lambda} \\
a &= (Z - 80)\alpha,
\end{aligned} \tag{5}$$

which was obtained from fitting radiative shifts for high Coulomb s-levels, in order to account for the potential near the core. Starting from a free-particle formulation, the potential would otherwise not be suited for small distances in heavy atoms $Z > 80$ [49, 56, 57]. Thierfelder and Schwerdtfeger [29] introduced the expression

$$A_n(Z) = A_{n0} + A_{n1} \frac{Z}{1 + \exp \left[(Z/A_{n2})^5 \right]} \tag{6}$$

depending on the main quantum number n and the values of A_{ni} were obtained from fitting self energy contributions to H-like atoms, calculated by Mohr [20, 56–58]. Multiplied with the cut-off term $\Theta(Z, r)$, this gives another prefactor, which is important for comparing results. Finally, the low frequency contribution

$$V_l(\vec{r})/E_h = B(Z)Z^4\alpha^3 e^{-\frac{Z|\vec{r}|}{a_0}} \tag{7}$$

includes a fitting function

$$B(Z) = 0.074 + 0.35Z\alpha \tag{8}$$

which reproduces radiative shifts for the high Coulomb p-levels [56, 57]. Flambaum and Ginges chose it to be in the range of the size of the 1s orbital a_0/Z [49].

C. Perturbative computation of QED corrections

As QED corrections are always small compared to the total energy, it is generally sufficient to include them perturbatively. For a variational wave function the QED correction can be simply obtained as expectation value of the QED potential

$$\Delta E_{\text{QED}} = \langle \Psi | V_{\text{VP}} + V_{\text{SE}} | \Psi \rangle, \tag{9}$$

where closed expression for the VP and SE corrections to the potential energy V_{VP} , V_{SE} are given above. Note that non-local SE corrections as e.g. suggested in Ref. [30], would require a perturbative correction of the wave function as well.

In a mean-field approach based on the expansion of the Hilbert space in a set of molecular orbitals ψ_i , which are represented as linear combination of Gaussian basis functions χ_μ , $\psi_i = \sum_\mu C_{\mu i} \chi_\mu$ with the molecular orbital or Kohn-Sham orbital coefficients $C_{\mu i}$, the QED correction to the total energy is then obtained as the sum over all occupied orbital contributions i

$$\Delta E_{\text{QED}} = \sum_i \langle \psi_i | V_{\text{VP}} + V_{\text{SE}} | \psi_i \rangle \tag{10}$$

In such a mean-field approach, first order corrections to orbital energies ϵ_i require the evaluation of the linearly perturbed Fock matrix i.e.

III. METHODS

A. Cubic spline interpolation

The Uehling potential was implemented for a point-like nucleus following the approach by Fullerton and Rinker [46]. The Pyykkö–Zhao potential as well as the low frequency contribution to the Flambaum–Ginges potential contain analytically solvable integrals and, therefore, could be directly implemented as operators on a grid (following Ref. [60]) according to equations (2) and (7). To our knowledge no closed-form for the integrals appearing in the magnetic (3) and high frequency (4) contributions to the Flambaum–Ginges potential exist. Therefore, we approximated these integrals with the help of cubic spline interpolation. For this purpose, the integral was evaluated numerically on a grid using Mathematica 11.01 [62]. The two integrals have finite values for $r \rightarrow 0$ and approach zero for $r \rightarrow \infty$. They are approximated with cubic spline interpolation based on 1000 logarithmically spaced grid points in the range of $10^{-10} < r/a_0 < 0.1$ each. The first grid point was chosen to be this small, because the effective potentials probe the electronic structure at the vicinity of the nucleus. The mean relative errors of the spline compared to the numerically obtained values at 10000 equidistant points in the same range is 1.00×10^{-5} . A similar approach was taken for the integral in the high frequency contribution. In order to exclude the nuclear charge Z from the cubic spline interpolation, the integral was written as

$$\begin{aligned} & \int_1^\infty \frac{e^{-\frac{2t|\vec{r}|}{\lambda}}}{\sqrt{t^2-1}} \left[\left(1 - \frac{1}{2t^2}\right) \right. \\ & \times \left. \left(\ln(t^2-1) + 4 \ln\left(\frac{1}{Z\alpha} + \frac{1}{2}\right) \right) + \frac{1}{t^2} - \frac{3}{2} \right] dt \\ & = 4 \ln\left(\frac{1}{Z\alpha} + \frac{1}{2}\right) \int_1^\infty \frac{e^{-\frac{2t|\vec{r}|}{\lambda}}}{\sqrt{t^2-1}} \left(1 - \frac{1}{2t^2}\right) dt \\ & + \int_1^\infty \frac{e^{-\frac{2t|\vec{r}|}{\lambda}}}{\sqrt{t^2-1}} \left[\left(1 - \frac{1}{2t^2}\right) \ln(t^2-1) + \frac{1}{t^2} - \frac{3}{2} \right] dt \end{aligned} \quad (15)$$

Just as for the magnetic contribution, the two integrals trend to finite values for $r \rightarrow 0$ and to zero for $r \rightarrow \infty$. Cubic spline interpolation based on 1500 logarithmically spaced grid points in the range of $10^{-10} < r/a_0 < 0.1$ yielded a mean relative error of $< 6.70 \times 10^{-5}$ compared to the numerically obtained values at 10000 equidistant points in the same range. Further documentation can be found in the supporting information.

B. Computational details

All calculations were performed using a modified version [40, 59, 60, 63–66] of a quasi-relativistic program package

$$\Delta\epsilon_{i,\text{QED}} = \langle \psi_i | V_{\text{VP}} + V_{\text{SE}} | \psi_i \rangle + G_{ii}(\mathbf{D}'_{\text{QED}}). \quad (11)$$

The first order perturbed two-electron matrix \mathbf{G} is defined as

$$G_{ii} = \sum_{\mu\nu\rho\sigma} C_{\mu i}^\dagger C_{\nu i} \left[D'_{\text{QED},\rho\sigma} \left((\mu\nu|\rho\sigma) - a_X \frac{1}{2} (\mu\sigma|\rho\nu) \right) + a_{\text{DFT}} \langle \chi_\mu | V'_{\text{XC}}(\mathbf{D}, \mathbf{D}'_{\text{QED}}) | \chi_\nu \rangle \right] \quad (12)$$

where the Mulliken notation for two electron integrals is employed: $(\mu\nu|\rho\sigma) = \iint d^3r_1 d^3r_2 \chi_\mu(\vec{r}_1) \chi_\rho(\vec{r}_2) \frac{1}{|\vec{r}_1 - \vec{r}_2|} \chi_\nu(\vec{r}_1) \chi_\sigma(\vec{r}_2)$, \mathbf{D} is the density matrix with elements $D_{\mu\nu} = \sum_i n_i C_{\mu i}^\dagger C_{\nu i}$, with the occupation vector \vec{n} and the linearly perturbed density matrix \mathbf{D}'_{QED} being obtained from the linear response of ψ_i or \mathbf{D} to the QED potentials as described in Ref. [59]. In case of pure DFT (non-hybrid) we have $a_X = 0$ and in case of pure HF we have $a_X = 1$ and $a_{\text{DFT}} = 0$. V'_{XC} is the perturbed exchange-correlation potential.

D. Picture-change transformation within ZORA

All QED potentials discussed in this work are one-electron operators. Therefore, all four-component representations of these potentials given in the previous sections can be transformed to two-component form within zeroth order regular approximation (ZORA) using the approach and implementation detailed in Ref. [60]. Here we implicitly generate the small component within ZORA from the ZORA wave function as:

$$\psi^{\text{S}} \approx \psi_{\text{ZORA}}^{\text{S}} = \frac{c}{2m_e c^2 - \bar{V}} \vec{\sigma} \cdot \vec{p} \psi_{\text{ZORA}} \quad (13)$$

For this purpose we employ the model potential \tilde{V} formulation of ZORA by van Wüllen [61]. For details on how resulting matrix elements are derived and computed see Ref. [60]. If not stated explicitly otherwise we include picture-change corrections due to a different normalisation of the wave function in a four component framework by applying a renormalisation of ZORA spinors as follows:

$$\psi_i^{\text{rZORA}} = \frac{\psi_i^{\text{ZORA}}}{\sqrt{1 + \langle \psi_{i,\text{ZORA}}^{\text{S}} | \psi_{i,\text{ZORA}}^{\text{S}} \rangle}} \quad (14)$$

Response calculations and corrections of orbital energies were computed as detailed in Refs. [40, 59].

[67] based on Turbomole [68]. If not stated otherwise, the two-component wave functions were obtained from a complex Generalised Hartree–Fock (cGHF) calculation using the ZORA [69–72] framework, employing a model potential to alleviate the gauge dependence of ZORA as suggested by van Wüllen [61]. The model potential was applied with additional damping of the atomic Coulomb contribution to the model potential [73]. The nuclei were modelled using normalised spherical Gaussian nuclear density distributions $\varrho_A(\vec{r}) = \frac{\zeta_A^{3/2}}{\pi^{3/2}} e^{-\zeta_A|\vec{r}-\vec{r}_A|^2}$ with $\zeta_A = \frac{3}{2r_{\text{nuc},A}^2}$ for the Coulomb part of the electron-nucleus potential. The root-mean-square radius $r_{\text{nuc},A}$ was chosen as suggested by Visscher and Dyall [74]. Wave functions were converged until the energy change between two consecutive self-consistent field cycles was below $10^{-12}E_h$. In subsequent computations of QED contributions, a point-like nucleus was used. The basis sets, which were used for the various calculations, are all specified in the related tables. The contributions to the orbital energies of gold in Table V were calculated using the Becke 3-parameters hybrid exchange functional with the correlation functional by Lee, Yang and Parr (B3LYP) [75–80]. For the perturbative treatment of QED corrections reported in Table V, the response calculation was converged to $10^{-9}E_h$. For a better comparison to the work of Thierfelder and Schwerdtfeger, the results of Tables I, II and III were obtained using the factor of equation (6) in the high-frequency contribution to the Flambaum–Ginges effective potential. For all other calculations, the factor by Flambaum and Ginges (5) was used. If not stated otherwise, the following isotopes were used: ^4_2He , ^7_3Li , ^9_4Be , $^{11}_5\text{B}$, $^{20}_{10}\text{Ne}$, $^{23}_{11}\text{Na}$, $^{24}_{12}\text{Mg}$, $^{27}_{13}\text{Al}$, $^{40}_{18}\text{Ar}$, $^{39}_{19}\text{K}$, $^{40}_{20}\text{Ca}$, $^{64}_{28}\text{Cu}$, $^{65}_{30}\text{Zn}$, $^{70}_{31}\text{Ga}$, $^{84}_{36}\text{Kr}$, $^{85}_{37}\text{Rb}$, $^{88}_{38}\text{Sr}$, $^{91}_{40}\text{Zr}$, $^{108}_{47}\text{Ag}$, $^{112}_{48}\text{Cd}$, $^{115}_{49}\text{In}$, $^{119}_{50}\text{Sn}$, $^{131}_{54}\text{Xe}$, $^{133}_{55}\text{Cs}$, $^{137}_{56}\text{Ba}$, $^{144}_{60}\text{Nd}$, $^{173}_{70}\text{Yb}$, $^{197}_{79}\text{Au}$, $^{201}_{80}\text{Hg}$, $^{204}_{81}\text{Tl}$, $^{222}_{86}\text{Rn}$, $^{223}_{87}\text{Fr}$, $^{226}_{88}\text{Ra}$, $^{232}_{90}\text{Th}$. Relative deviations (in percent) as denoted in the various tables as Dev. were calculated according to $100 \times |(X - X_{\text{lit}})/X_{\text{lit}}|$, where X corresponds to our computed value and X_{lit} to the corresponding literature value we compare to.

IV. RESULTS AND DISCUSSION

A. Ionisation energies

QED contributions to the ionisation energies of group 1, 2, 11, 12, 13 and 18 atoms are listed in Table I. SE and VP show opposite sign and grow larger in magnitude with increasing nuclear charge Z . For atoms up to the fifth period of the periodic table, the absolute value of the vacuum polarisation contribution is roughly one order of magnitude smaller than that of the electron self energy term. In the case of higher nuclear charges, $Z > 80$, the vacuum polarisation contributes to the same order of magnitude. The two contributions essentially cancel each other out at one point, after which the VP will be greater in magnitude than the SE. The largest

TABLE I: SE (Flambaum–Ginges) and VP (Uehling) contributions in eV to the ionisation energies of group 1, 2, 11, 12, 13 and 18 atoms, calculated as expectation values based on ZORA-HF/dyall.ae4z calculations, using prefactor (6). Comparison [29] with four-component DHF calculations with perturbative treatment of the QED contributions.

	V_{SE}	V_{VP}	Dev./%	Dev./%
Li	-3.372×10^{-5}	1.178×10^{-6}	0.1	0.9
Na	-3.051×10^{-4}	1.628×10^{-5}	0.3	0.5
K	-5.486×10^{-4}	3.724×10^{-5}	0.1	0.2
Rb	-1.452×10^{-3}	1.443×10^{-4}	0.7	0.3
Cs	-2.389×10^{-3}	3.299×10^{-4}	0.5	0.5
Fr	-6.392×10^{-3}	1.614×10^{-3}	2.1	1.8
Be ^a	-9.019×10^{-5}	3.420×10^{-6}	0.2	0.9
Be ^b	-8.044×10^{-5}	3.046×10^{-6}	11.2	12.4
Mg	-4.424×10^{-4}	2.438×10^{-5}	0.3	1.3
Ca	-6.873×10^{-4}	4.775×10^{-5}	1.5	1.7
Sr	-1.678×10^{-3}	1.692×10^{-4}	1.6	2.1
Ba	-2.666×10^{-3}	3.724×10^{-4}	2.3	2.4
Ra	-6.842×10^{-3}	1.743×10^{-3}	2.0	2.6
Cu	-3.363×10^{-3}	2.769×10^{-4}	1.1	0.1
Ag	-7.420×10^{-3}	8.505×10^{-4}	0.6	0.2 ^b
Au	-2.661×10^{-2}	5.294×10^{-3}	0.7	0.2
Zn	-3.342×10^{-3}	2.818×10^{-4}	0.7	1.6
Cd	-7.209×10^{-3}	8.434×10^{-4}	1.1	1.5
Hg	-2.566×10^{-2}	5.214×10^{-3}	0.3	0.9
B	2.365×10^{-4}	-9.815×10^{-6}	0.7	1.2
Al	5.741×10^{-4}	-3.323×10^{-5}	0.6	3.5
Ga	2.130×10^{-3}	-1.798×10^{-4}	5.6	5.3
In	3.657×10^{-3}	-4.230×10^{-4}	5.5	5.5
Tl	6.530×10^{-3}	-1.282×10^{-3}	4.9	4.6
He	-1.776×10^{-4}	5.802×10^{-6}	0.3	1.2
Ne	1.032×10^{-3}	-5.982×10^{-5}	4.0	5.2
Ar	1.209×10^{-3}	-9.296×10^{-5}	4.0	5.2
Kr	2.285×10^{-3}	-2.908×10^{-4}	2.9	4.4
Xe	2.997×10^{-3}	-5.899×10^{-4}	2.8	4.0
Rn	5.622×10^{-3}	-2.260×10^{-3}	0.7	3.3

^a Restricted Hartree–Fock (RHF) solution ^b Lower energy broken-symmetry solution with deviations higher than those of the RHF solution, which agrees excellently with the literature. ^c Deviation obtained from a corrected four-component VP contribution of 8.492×10^{-4} eV, instead of 8.930×10^{-4} eV as obtained previously in Ref. 29. The latter resulted from a minor deficiency in a GRASP routine that assumed a VP large-distance limit to be reached once, for some distance, deviations between asymptotic expansion and explicit computation fall below a given threshold. Here, however, curves crossed rather than merged so that a grid point coincidentally hitting this crossing flagged erroneously an arrival in the large-distance regime.

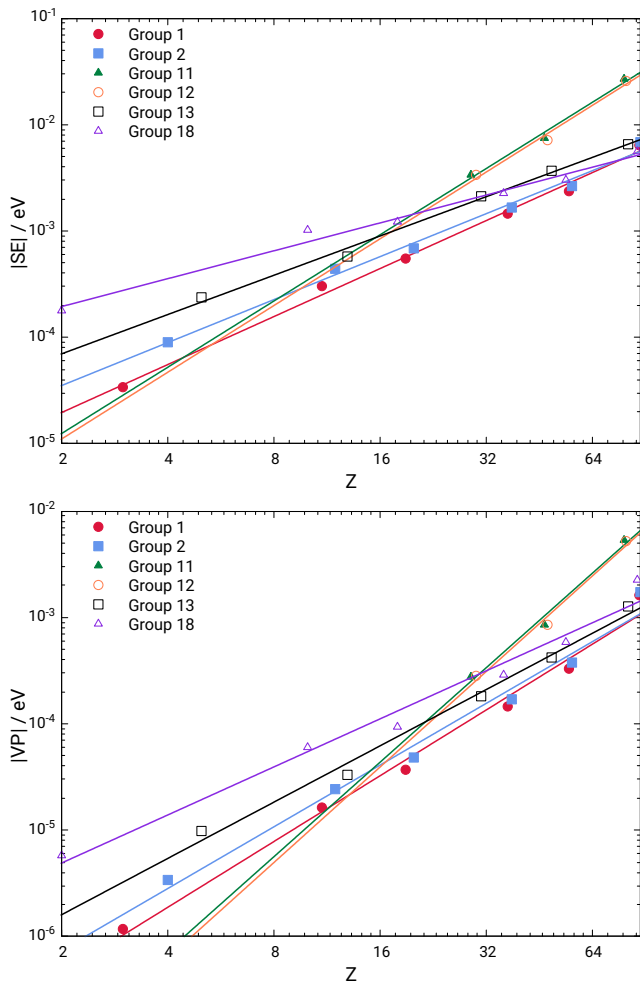


FIG. 3: Absolute SE (Flambaum-Ginges) and VP (Uehling) contributions to the ionisation energies of group 1, 2, 11, 12 and 18 atoms from Table I with linear fits in a log-log scale plot.

absolute values of SE contributions were found for Au and Hg, followed by their lighter group homologues Ag and Cd. The smallest contributions, in magnitude, were computed for Li and Be. The strongest VP contributions were also found for Au and Hg, followed by Rn and Ra. The weakest contributions were again obtained for Li and Be. To determine the scaling of QED contributions to the ionisation energies with Z , we plotted them with logarithmic scales on abscissa and ordinate in Figure 3. Linear fits for each considered group of the periodic table of elements yielded the parameters in Table II. The VP shows generally larger exponents B , which is in accordance with the results obtained. QED contributions grow faster with increasing nuclear charge for groups 11 and 12, which points at the already known relative maximum of relativistic effects at group 11 [9]. Deviations of scaling parameters from those reported by Thierfelder and Schwerdtfeger stem from the exclusion of super-heavy elements in our present work.

TABLE II: Scaling parameters for the SE (Flambaum-Ginges) and VP (Uehling) contributions to ionisation energies of atoms, sorted by groups according to AZ^B , obtained from linear regression of the results in Table I, shown in Figure 3.

Group	A_{SE}	B_{SE}	A_{VP}	B_{VP}
1	6.913×10^{-6}	1.499	1.084×10^{-7}	2.054
2	1.383×10^{-5}	1.342	1.942×10^{-7}	1.928
11	2.953×10^{-6}	2.069	1.205×10^{-8}	2.952
12	2.595×10^{-6}	2.084	9.942×10^{-9}	2.983
13	2.977×10^{-5}	1.227	4.715×10^{-7}	1.758
18	1.063×10^{-4}	0.870	1.727×10^{-6}	1.501

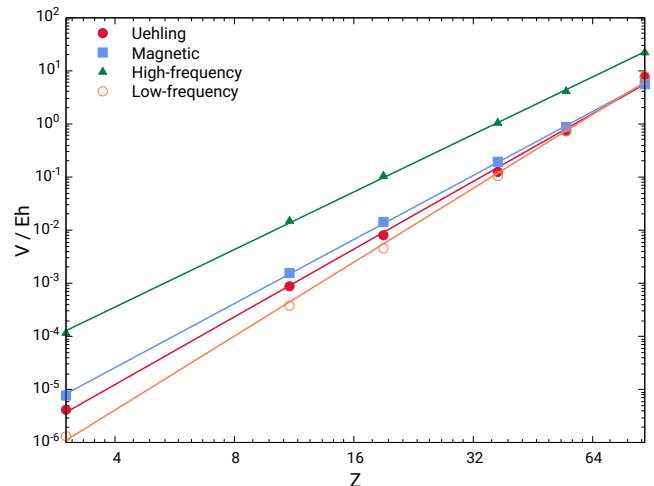


FIG. 4: Absolute SE (Flambaum-Ginges) and VP (Uehling) contributions to the energies of group 1 atoms from Table (IX) and (X) with linear fits in a log-log scale plot.

Contributions to ionisation energies of group 1 and 2 atoms agree excellently with the four-component DHF calculations by Thierfelder and Schwerdtfeger [29] with deviations remaining in the range of 0.1–2.6%. For Be, the first result shows a deviation of 0.2% for the SE and 0.9% for the VP. In addition, we obtained another Hartree-Fock solution for Be, which is $3.2 \times 10^{-4} E_h$ lower in total energy. Using the energetically lower wave function for the neutral Be atom, the SE contribution weakens to $-8.044 \times 10^{-5} \text{ eV}$ and shows a deviation of 11.2%, while the VP is lowered to $3.046 \times 10^{-6} \text{ eV}$ with a deviation of 12.4%. The first result, which is in agreement with the literature value [29] is an RHF solution, while the second result is a GHF solution. Groups 11 and 12 show deviations of only 0.1–1.6% from four-component results, whereas Groups 13 and 18 atoms show deviations of 0.3–5.6%. Except for helium, which also gives opposite signs compared to the rest of the group 13 and 18 atoms, an ionisation of the p-shell instead of the s-shell was considered.

For group 13 the electron was removed from the $p_{1/2}$ and

TABLE III: SE (Flambaum–Ginges) and VP (Uehling) contributions in eV to the ${}^2P_{1/2} \leftarrow {}^2S_{1/2}$ and ${}^2P_{3/2} \leftarrow {}^2S_{1/2}$ transitions calculated as expectation values based on ZORA-HF/dyall.cv3z calculations, using prefactor (6). Comparison [29] with four-component numerical DHF calculations with perturbative treatment of the QED contributions. Z is the nuclear charge and N is the number of electrons.

Z	N	$V_{SE,2P1/2}$	$V_{SE,2P3/2}$	Dev./%	Dev./%	$V_{VP,2P1/2}$	$V_{VP,2P3/2}$	Dev./%	Dev./%
10	3	-1.498×10^{-2}	-1.436×10^{-2}	0.0	0.0	7.643×10^{-4}	7.643×10^{-4}	0.0	0.0
20	3	-2.065×10^{-1}	-1.936×10^{-1}	0.5	0.0	1.414×10^{-2}	1.417×10^{-2}	1.4 ^a	0.7 ^b
30	3	-8.864×10^{-1}	-8.179×10^{-1}	0.1	0.1	7.562×10^{-2}	7.616×10^{-2}	0.7	0.7
40	3	-2.448	-2.238	0.3	0.4	2.526×10^{-1}	2.568×10^{-1}	0.4	0.4
50	3	-5.379	-4.906	0.5	0.6	6.631×10^{-1}	6.838×10^{-1}	0.3	0.2
60	3	-1.032×10^1	-9.467	1.1	1.0	1.513	1.591	0.1	0.3
70	3	-1.810×10^1	-1.691×10^1	1.1	1.3	3.169	3.420	0.4	0.6
80	3	-2.988×10^1	-2.885×10^1	1.2	1.6	6.293	7.040	0.5	0.9
90	3	-4.725×10^1	-4.802×10^1	0.9	1.5	1.213×10^1	1.424×10^1	0.0	0.6
20	11	-2.916×10^{-2}	-2.752×10^{-2}	0.0	0.0	1.965×10^{-3}	1.968×10^{-3}	0.0	0.0
30	11	-1.736×10^{-1}	-1.611×10^{-1}	0.0	0.0	1.450×10^{-2}	1.459×10^{-2}	0.7	0.7
40	11	-5.457×10^{-1}	-5.014×10^{-1}	0.0	0.2	5.484×10^{-2}	5.578×10^{-2}	0.9	0.9
50	11	-1.285	-1.177	0.1	0.0	1.534×10^{-1}	1.585×10^{-1}	1.3	1.3
80	11	-7.764	-7.454	0.5	0.3	1.555	1.760	1.5	1.1
90	11	-1.239×10^1	-1.241×10^1	1.1	0.8	2.999	3.584	2.4	1.7
40	29	-7.905×10^{-2}	-7.322×10^{-2}	0.1	0.0	7.893×10^{-3}	8.005×10^{-3}	1.3	1.2
50	29	-2.658×10^{-1}	-2.445×10^{-1}	0.0	0.2	3.146×10^{-2}	3.240×10^{-2}	0.9	0.9
60	29	-6.316×10^{-1}	-5.826×10^{-1}	0.2	0.0	8.837×10^{-2}	9.299×10^{-2}	1.0	0.9
70	29	-1.259	-1.177	0.3	0.1	2.088×10^{-1}	2.263×10^{-1}	1.0	0.9
90	29	-3.762	-3.749	1.1	0.6	8.990×10^{-1}	1.073	2.1	1.5

^a Deviation from a four-component value of 1.42559×10^{-2} eV, which corrects a misprint in Ref. 29.

^b Deviation from a four-component value of 1.42905×10^{-2} eV, which corrects a misprint in Ref. 29.

TABLE IV: SE (Flambaum–Ginges) and VP (Uehling) contributions in eV to the valence orbital energies of group 1 and 11 atoms calculated as expectation values based on ZORA-HF/dyall.v3z, using prefactor (5). Comparison [38] with four-component AOC-HF/dyall.v3z calculations based on DC Hamiltonians.

	V_{SE}	V_{VP}	Dev./%	Dev./%
Li	4.024×10^{-5}	-1.350×10^{-6}	1.7	1.7
Na	2.934×10^{-4}	-1.527×10^{-5}	0.5	0.6
K	5.133×10^{-4}	-3.406×10^{-5}	0.4	0.5
Rb	1.359×10^{-3}	-1.307×10^{-4}	0.2	0.2
Cs	2.305×10^{-3}	-2.989×10^{-4}	0.0	0.0
Fr	6.385×10^{-3}	-1.452×10^{-3}	0.8	1.0
Cu	2.851×10^{-3}	-2.363×10^{-4}	0.4	0.3
Ag	6.464×10^{-3}	-7.356×10^{-4}	0.3	0.2
Au	2.374×10^{-2}	-4.637×10^{-3}	0.0	0.0

for group 18 from the $p_{3/2}$ orbitals. Extensive data on converged wave functions for different ionisations can be found in the supporting information. It is worth noting, that the high-frequency part of the Flambaum–Ginges potential causes the (in magnitude) largest contribution to the SE ($\approx 59\%$ for Au, $\approx 71\%$ for Ag, $\approx 79\%$ for Cu) and claims an even greater share of the contribution

to the ionisation energy ($\approx 70\%$ for Au, $\approx 78\%$ for Ag, $\approx 82\%$ for Cu). Consequently, the prefactor (6), introduced by Thierfelder and Schwerdtfeger, is important to consider when comparing results. When neglected, the computed QED corrections show greater deviations from the four-component data. As it scales with Z^4 , the low-frequency contribution to the ionisation energies grows from $\approx 4.4\%$ for Cu, over $\approx 6.9\%$ for Ag, to $\approx 13.2\%$ for Au. The magnetic contribution shows a smaller increase ($\approx 16.4\%$ for Au, $\approx 15.3\%$ for Ag, $\approx 13.1\%$ for Cu).

B. Electronic transition energies

SE and VP contributions to ${}^2P_{1/2} \leftarrow {}^2S_{1/2}$ and ${}^2P_{3/2} \leftarrow {}^2S_{1/2}$ transition energies of Li-, Na- and Cu-like ions with nuclear charges $Z = 10, 20, \dots, 90$ are listed in Table III. As observed for the contributions to the ionisation energies, the SE and VP show opposite sign, with SE being roughly one order of magnitude larger in absolute value than the VP. Comparing the same elements, Li-like ions show larger contributions to the transition energies than the corresponding Na- and Cu-like ions. This aligns with the general trend of the transition energies, which for Li-like ions exceed those of Cu-like ions by far. Ex-

TABLE V: Perturbative and self-consistent QED contributions in E_h to the Kohn–Sham orbital energies of gold, calculated on ZORA-B3LYP/dyall.3zp level of theory, using prefactor (5) and deviation from self-consistent four-component B3LYP/dyall.3zp calculations of Ref. [38] (Dev.). FG is the Flambaum–Ginges, PZ the Pyykkö–Zhao and UE the Uehling potential.

	Perturbative		Self-consistent			
	V_{FG+UE}^a	V_{PZ+UE}^a	V_{FG+UE}^a	Dev./%	V_{PZ+UE}^a	Dev./%
1s _{1/2}	8.285	8.279	8.262	29.6	8.267	32.4
2s _{1/2}	8.991×10^{-1}	9.109×10^{-1}	8.967×10^{-1}	6.1	9.098×10^{-1}	6.0
2p _{1/2}	6.656×10^{-2}	6.668×10^{-2}	6.796×10^{-2}	15.3	6.777×10^{-2}	13.8
2p _{3/2}	1.265×10^{-1}	-3.211×10^{-2}	1.275×10^{-1}	6.8	-3.124×10^{-2}	2.3
3s _{1/2}	1.912×10^{-1}	1.968×10^{-1}	1.907×10^{-1}	2.4	1.965×10^{-1}	2.1
3p _{1/2}	7.968×10^{-3}	1.548×10^{-2}	8.215×10^{-3}	12.2	1.566×10^{-2}	7.1
3p _{3/2}	2.251×10^{-2}	-8.719×10^{-3}	2.269×10^{-2}	2.5	-8.564×10^{-3}	0.6
3d _{3/2}	-1.445×10^{-2}	-9.181×10^{-3}	-1.441×10^{-2}	0.8	-9.168×10^{-3}	0.9
3d _{5/2}	-5.968×10^{-3}	-8.759×10^{-3}	-5.930×10^{-3}	1.9	-8.751×10^{-3}	1.9
4s _{1/2}	4.732×10^{-2}	4.897×10^{-2}	4.717×10^{-2}	1.4	4.889×10^{-2}	1.2
4p _{1/2}	1.254×10^{-3}	3.507×10^{-3}	1.297×10^{-3}	15.4	3.531×10^{-3}	5.9
4p _{3/2}	4.695×10^{-3}	-2.449×10^{-3}	4.722×10^{-3}	1.5	-2.429×10^{-3}	0.1
4d _{3/2}	-3.435×10^{-3}	-2.293×10^{-3}	-3.441×10^{-3}	0.2	-2.308×10^{-3}	0.0
4d _{5/2}	-1.659×10^{-3}	-2.188×10^{-3}	-1.667×10^{-3}	1.2	-2.203×10^{-3}	0.8
5s _{1/2}	9.149×10^{-3}	9.541×10^{-3}	9.105×10^{-3}	1.1	9.508×10^{-3}	0.8
4f _{5/2}	-2.385×10^{-3}	-1.450×10^{-3}	-2.403×10^{-3}	0.8	-1.472×10^{-3}	0.8
4f _{7/2}	-1.828×10^{-3}	-1.416×10^{-3}	-1.847×10^{-3}	1.3	-1.438×10^{-3}	0.9
5p _{1/2}	-1.139×10^{-5}	4.545×10^{-4}	-1.654×10^{-5}	63.8	4.440×10^{-4}	8.2
5p _{3/2}	5.803×10^{-4}	-5.556×10^{-4}	5.726×10^{-4}	1.9	-5.666×10^{-4}	0.7
5d _{3/2}	-4.480×10^{-4}	-3.274×10^{-4}	-4.568×10^{-4}	2.0	-3.391×10^{-4}	2.7
5d _{5/2}	-2.758×10^{-4}	-3.041×10^{-4}	-2.874×10^{-4}	0.2	-3.185×10^{-4}	0.7
6s _{1/2}	7.226×10^{-4}	7.460×10^{-4}	7.190×10^{-4}	10.3	7.399×10^{-4}	10.0

^a In case two different values were obtained in the cGHF framework for a Kramers pair, contributions were averaged.

TABLE VI: SE (Flambaum–Ginges) contributions in E_h to Hartree–Fock orbital energies of selected atoms calculated as expectation values based on ZORA-HF/dyall.ae4z calculations, using prefactor (5) and comparison to results by Koziol and Aucar [81].

	Zn		Cd		Hg	
	V_{SE}	Ref. ^a	V_{SE}	Ref. ^a	V_{SE}	Ref. ^a
1s _{1/2}	2.834×10^{-1}	2.466×10^{-1}	1.499	1.220	1.007×10^1	7.408
2s _{1/2}	2.710×10^{-2}	2.613×10^{-2}	1.587×10^{-1}	1.501×10^{-1}	1.218	1.130
2p _{1/2}	-1.385×10^{-4}	-4.740×10^{-4}	3.917×10^{-3}	-2.000×10^{-5}	1.626×10^{-1}	9.397×10^{-2}
2p _{3/2}	1.778×10^{-3}	1.180×10^{-3}	1.618×10^{-2}	1.114×10^{-2}	1.857×10^{-1}	1.296×10^{-1}
3s _{1/2}	3.870×10^{-3}	3.815×10^{-3}	2.991×10^{-2}	2.920×10^{-2}	2.686×10^{-1}	2.615×10^{-1}
3p _{1/2}	-2.387×10^{-5}	-3.700×10^{-5}	6.096×10^{-4}	3.200×10^{-4}	3.293×10^{-2}	2.689×10^{-2}
3p _{3/2}	2.142×10^{-4}	1.500×10^{-4}	2.784×10^{-3}	2.110×10^{-3}	3.893×10^{-2}	3.112×10^{-2}
3d _{3/2}	-2.042×10^{-5}	-7.000×10^{-6}	-2.660×10^{-4}	-1.700×10^{-4}	-1.201×10^{-3}	-1.830×10^{-3}
3d _{5/2}	2.295×10^{-5}	7.000×10^{-6}	4.627×10^{-4}	2.100×10^{-4}	7.009×10^{-3}	3.690×10^{-3}
4s _{1/2}	1.588×10^{-4}	1.600×10^{-4}	5.354×10^{-3}	5.281×10^{-3}	6.681×10^{-2}	6.589×10^{-2}
4p _{1/2}			9.495×10^{-5}	6.600×10^{-5}	7.833×10^{-3}	6.854×10^{-3}
4p _{3/2}			4.345×10^{-4}	3.300×10^{-4}	9.186×10^{-3}	7.493×10^{-3}
4d _{3/2}			-2.462×10^{-5}	-1.000×10^{-5}	-1.199×10^{-4}	-2.700×10^{-4}
4d _{5/2}			4.665×10^{-5}	2.000×10^{-5}	1.585×10^{-3}	7.310×10^{-4}

^a Additional digits, exceeding those reported in Ref. 81, were provided by K. Koziol in personal communication.

TABLE VII: SE (Flambaum–Ginges) and VP (Uehling) contributions in eV to the ionisation energies of group 2 monofluorides calculated as expectation values based on ZORA-HF/dyall.cv3z calculations, using prefactor (5). The bond lengths for the neutral molecule r_0 and the ion r_+ are in pm.

	r_0	r_+	V_{FG}	V_{UE}
BeF	135.39	130.10	-1.470×10^{-5}	-2.406×10^{-7}
MgF	173.63	167.26	-3.422×10^{-4}	1.878×10^{-5}
CaF	198.01	189.49	-6.285×10^{-4}	4.358×10^{-5}
SrF	210.26	201.66	-1.638×10^{-3}	1.631×10^{-4}
BaF	220.51	211.95	-2.834×10^{-3}	3.816×10^{-4}
RaF	227.73	219.43	-7.274×10^{-3}	1.787×10^{-3}

TABLE VIII: SE (Flambaum–Ginges) and VP (Uehling) contributions in cm^{-1} to the transition energies of BaF and RaF calculated as expectation values based on ZORA-HF/dyall.cv3z calculations, using prefactor (5).

	$\Pi_{1/2} \leftarrow \Sigma_{1/2}$		$\Pi_{3/2} \leftarrow \Sigma_{1/2}$	
	BaF	RaF	BaF	RaF
cGHF	1.156×10^4	1.270×10^4	1.211×10^4	1.432×10^4
VP	3.505	1.503×10^1	3.562	1.605×10^1
SE	-2.648×10^1	-6.172×10^1	-2.543×10^1	-6.243×10^1
QED	-2.297×10^1	-4.690×10^1	-2.187×10^1	-4.637×10^1
Total	1.154×10^4	1.265×10^4	1.209×10^4	1.428×10^4

cept for the case of Th^{87+} , the SE contributions to the ${}^2P_{1/2} \leftarrow {}^2S_{1/2}$ transition energies are larger in magnitude than the ones to the ${}^2P_{3/2} \leftarrow {}^2S_{1/2}$ transitions, although the transition energy itself is much smaller in the ${}^2P_{1/2} \leftarrow {}^2S_{1/2}$ case. Without the exception for Th^{87+} , the trend is the opposite for the VP. Here, the contributions to the ${}^2P_{3/2} \leftarrow {}^2S_{1/2}$ transition energies are always larger. The values obtained in the current work are compared to four-component DHF calculations by Thierfelder and Schwerdtfeger [29]. Our present SE contributions deviate from these by only 0.0–1.6%, while the VP contributions differ by 0.0–2.4%. As for the comparison of the contributions to the ionisation energies in the previous section, it was crucial to use the prefactor of equation (6). The most pronounced QED contributions of Table III are the ones to the ${}^2P_{1/2} \leftarrow {}^2S_{1/2}$ transition in Th^{87+} , where they amount to ≈ -35 eV. They constitute a significant correction to the ≈ 275 eV transition energy. Blundell [21] obtained a QED contribution to the ${}^2P_{1/2} \leftarrow {}^2S_{1/2}$ transition in Th^{87+} of -38.35 eV, lowering the transition energy from ≈ 309 eV to ≈ 271 eV.

C. Valence orbital energies

QED contributions to Hartree–Fock valence orbital energies of group 1 and 11 atoms are listed in Table IV. Again, VP and SE contributions show opposite signs and the VP is about one order of magnitude smaller in absolute value

TABLE IX: Scaling parameters for the SE (Flambaum–Ginges) and VP (Uehling) contributions to total energies of group one atoms calculated as expectation values based on ZORA-HF/dyall.cv3z calculations, using prefactor (5). The parameters, according to AZ^B , were obtained from linear regression, shown in Figure 4.

	V_u	V_m	V_h	V_l
A	3.560×10^{-8}	1.022×10^{-7}	2.464×10^{-6}	6.949×10^{-9}
B	4.226	3.996	3.591	4.612

TABLE X: SE (Flambaum–Ginges) contributions in E_h to the total energies of group 1 atoms, calculated as expectation values based on ZORA-HF/dyall.cv3z, using prefactor (5).

	V_u	V_m	V_h	V_l
Li	-4.137×10^{-6}	7.690×10^{-6}	1.144×10^{-4}	1.349×10^{-6}
Na	-8.871×10^{-4}	1.593×10^{-3}	1.515×10^{-2}	3.838×10^{-4}
K	-8.173×10^{-3}	1.403×10^{-2}	1.059×10^{-1}	4.606×10^{-3}
Rb	-1.265×10^{-1}	1.893×10^{-1}	1.058	1.036×10^{-1}
Cs	-7.158×10^{-1}	8.859×10^{-1}	4.147	7.220×10^{-1}
Fr	-7.505	5.565	2.151×10^1	8.001

than the SE. For gold, the QED corrections lift up the orbital energy of the HOMO by $\approx 0.25\%$. The values compare well to four-component average of configuration (AOC-HF) calculations reported by Sunaga, Salman and Saue [38]. Deviations range between 0.0% and 1.7%, although a different HF method was used. Overall, it was observed, that the choice of the basis set and resolution of the integration grid had a larger effect on the results than the level of theory.

On the density functional theory level, individual QED contributions to Kohn–Sham orbital energies of gold are listed in Table V. The perturbative and self-consistent treatment of the Flambaum–Ginges and Uehling (FG+UE), as well as the Pyykkö–Zhao and Uehling potentials (PZ+UE) are compared. In case of two different values for the Kramers pair in the cGHF frame, the orbital energy contributions have been averaged. The QED effects contribute mostly to the core orbitals and get smaller for the valence orbitals. Orbitals of higher angular momentum, such as d- and f-orbitals, show smaller contributions compared to s-orbitals of the same principal quantum number. In the perturbative treatment of the Pyykkö–Zhao and Uehling potentials, the contributions to the d- and f-orbitals are significantly smaller. This is the result of the SE potential, which is a simple Gaussian, including two fitting functions for s-levels [50]. For s-contributions, the Pyykkö–Zhao and Flambaum–Ginges give comparable results. However, for p-, d- and f-orbitals, the contributions differ significantly and also often show opposite signs. The values are compared to four-component calculations by Sunaga, Salman and Saue [38], who used the same density functional and basis set. Our results for the self-consistent inclusion of the QED contributions show deviations between 0.0–32.4% compared to the reference. In both cases, the very

first energy levels show larger deviations of 2.3–32.4%. These are caused by the energy shift of the ZORA Hamiltonian and mainly affect the first two energy levels. The $6s_{1/2}$ orbital contributions show deviations of 10.0% and 10.3%, which could be a result of the different open-shell treatments, which in our cGHF treatment account for spin-polarisation effects. The $np_{1/2}$ show higher deviations compared to the remaining p-, d- and f-level contributions. Especially the $5p_{1/2}$ of the Flambaum–Ginges contribution shows a large deviation of 63.8%. The origin of this deviation is presently open.

For comparison, QED corrections to Kohn-Sham orbital energies were also calculated perturbatively. As the corrections are relatively small, the two approaches, perturbative and self-consistent, are expected to yield comparable results. Sunaga *et al.*, however, reported noticeable differences between the two treatments on the orbital energy level. When comparing instead the total expectation value of the (sum of) one-electron operators, virtually identical results are obtained. If one accounts properly for the linear response as per Eq. 11, the differences between the two treatments become negligible also on the level of orbital energies. Only the $5p_{1/2}$ values stand out, because they show larger deviation between perturbative and self-consistent treatment of the Flambaum–Ginges term.

Another orbital contribution comparison is shown in Table VI. The SE contributions, evaluated as orbital expectation values (without response contributions), to group 12 atoms up to the 4d shell are compared to the results reported by Koziol and Aucar [81], who use a quite different approach to account for SE corrections (Welton picture). Nevertheless, the s-contributions compare well and show deviations up to 14.9% for the 1s level of Zn, 22.9% for Cd and 35.9% for the 1s level of Hg. The np and nd levels show larger deviations and in the case of $2p_{1/2}$ of Cd a different sign.

D. Total energies

Figure 4 shows QED contributions to the total energies of group 1 atoms due to the Uehling potential and the individual terms of the Flambaum–Ginges potential. Corresponding scaling parameters are listed in Table IX. The high-frequency contributions grows fastest, whereas the low-frequency term grows slowest with increasing the nuclear charge. The magnetic contribution scales higher than the Uehling potential. All of the terms scale much higher for the total energy contributions compared to the corrections to the ionisation energies of group one atoms of Table II.

E. Ionisation energies of group 2 monofluorides

QED contributions to the ionisation energies of group 2 monofluorides are listed in Table VII. The neutral

molecules, as well as the ions, were structurally optimised before QED corrections were included perturbatively. Equilibrium bond lengths obtained are reported in the table. While VP and SE show growing contributions with increasing nuclear charge Z of the metal atom, their sign is not always opposite to each other. In the case of BeF, VP and SE both show a negative sign. This is also the only case, in which the metal has a smaller nuclear charge than the fluoride. Besides that, the results are in accordance with general trends expected based on QED corrections for the corresponding group 2 atoms and agree also within 15 % with the very recently reported specific case of RaF for which a total QED correction of -6.4626 meV was obtained on the four-component Fock-space coupled cluster level [82].

F. Electronic transition energies of BaF and RaF

The QED contributions to the $\Pi_{1/2} \leftarrow \Sigma_{1/2}$ and $\Pi_{3/2} \leftarrow \Sigma_{1/2}$ transition energies of BaF and RaF are listed in Table VIII. In the case of BaF, 216.00 pm and 218.00 pm were chosen as bond length for the ground and excited state, respectively, of the molecule. For RaF, 223.84 pm was used for both states. The distances were chosen to provide a better comparison to the calculations of Skripnikov, Chubukov and Shakhova [37, 39, 83], who used them as well. The obtained QED contributions to the BaF transitions differ from the ones calculated by Skripnikov [37] by $\approx 23\%$ for the $\Pi_{1/2} \leftarrow \Sigma_{1/2}$ and $\approx 24\%$ for the $\Pi_{3/2} \leftarrow \Sigma_{1/2}$ transitions. The QED contributions to the transition energies of RaF differ from the ones calculated by Zaitsevskii *et al.* [39] by $\approx 16\%$ for the $\Pi_{1/2} \leftarrow \Sigma_{1/2}$ and $\approx 19\%$ for the $\Pi_{3/2} \leftarrow \Sigma_{1/2}$ transitions. The larger deviations between the values are attributed to the different formulation of the wave function and the SE. The latter’s share of the QED correction is larger than the one of the VP.

V. CONCLUSION

The Uehling potential, the Pyykkö–Zhao and the Flambaum–Ginges effective potentials have been implemented successfully in a two-component ZORA framework. For the Flambaum–Ginges potential, repeated numerical evaluation of integrals in the magnetic and high-frequency contributions, for which no analytical solution is available, was evaded by using cubic spline interpolation instead. Combined with the ZORA framework, this allows for fast evaluation of said QED corrections in atoms and molecules. The various exemplary calculations demonstrate the accuracy of this approach. Corrections to energy levels, ionisation energies and transition energies compare well to four-component numerical DHF calculations by Thierfelder and Schwerdtfeger [29] or four-component AOC-HF calculations by Sunaga,

Salman and Saue [38]. Here, it was observed, that the basis set had a greater impact on the QED corrections, than the level of theory alone. Furthermore, the contributions to the ionisation energies of group 2 monofluorides are presented. Overall, we find the impact of different schemes to account for electron self-energy corrections to be much larger than residual deviations between our present two-component ZORA framework and related four-component frameworks. The two-component scheme reported herein thus opens up an avenue to assess the role of QED corrections in atoms and larger molecules as well as to explore applicabilities and limitations of var-

ious approximate schemes to account for contributions from quantum electrodynamics to energies and molecular properties.

VI. ACKNOWLEDGEMENT

The authors thank G. A. Aucar, I. A. Aucar and K. Koziol for discussions and gratefully acknowledge K. Koziol as well as A. Kiuberis for sharing results with increased number of digits in personal communications. P. S. thanks Prof. P. Indelicato (Laboratoire Kastler Brossel, Sorbonne, Paris) for a visiting professorship.

-
- [1] P. Pyykkö, *Chem. Rev.* **88**, 563 (1988).
- [2] P. Pyykkö, *Chemical Reviews* **112**, 371 (2012).
- [3] P. A. M. Dirac, *Proc. Roy. Soc. Lond. A* **117**, 610 (1928).
- [4] P. A. M. Dirac, *Proc. Roy. Soc. Lond. A* **118**, 351 (1928).
- [5] T. Saue, *ChemPhysChem* **12**, 3077 (2011).
- [6] W. Greiner and J. Reinhardt, *Quantum Electrodynamics*, 4th ed. (Springer, 2009).
- [7] G. Breit, *Phys. Rev.* **34**, 553 (1929).
- [8] P. Indelicato, J. Bieroń, and P. Jönsson, *Theoretical Chemistry Accounts* **129**, 495 (2011).
- [9] P. Pyykkö, *Annu. Rev. Phys. Chem.* **63**, 45 (2012).
- [10] W. E. Lamb and R. C. Retherford, *Phys. Rev.* **72**, 241 (1947).
- [11] M. S. Safronova, D. Budker, D. DeMille, D. F. J. Kimball, A. Derevianko, and C. W. Clark, *Rev. Mod. Phys.* **90**, 025008 (2018).
- [12] R. Berger and J. Stohner, *Wiley Interdiscip. Rev.-Comput. Mol. Sci.* **9**, e1396 (2019).
- [13] T. A. Isaev, S. Hoekstra, and R. Berger, *Phys. Rev. A* **82**, 052521 (2010).
- [14] T. A. Isaev and R. Berger, *ArXiv e-prints* **1302.5682**, physics.chem (2013), arXiv:1302.5682 [physics.chem-ph].
- [15] L. P. Gaffney, P. A. Butler, M. Scheck, A. B. Hayes, F. Wenander, M. Albers, B. Bastin, C. Bauer, A. Blazhev, S. Bönig, N. Bree, J. Cederkäll, T. Chupp, D. Cline, T. E. Cocolios, T. Davinson, H. DeWitte, J. Diriken, T. Grahn, A. Herzan, M. Huyse, D. G. Jenkins, D. T. Joss, N. Kesteloot, J. Konki, M. Kowalczyk, T. Kröll, E. Kwan, R. Lutter, K. Moschner, P. Napiorkowski, J. Pakarinen, M. Pfeiffer, D. Radeck, P. Reiter, K. Reynders, S. V. Rigby, L. M. Robledo, M. Rudigier, S. Sambhi, M. Seidlitz, B. Siebeck, T. Stora, P. Thoele, P. Van Duppen, M. J. Vermeulen, M. von Schmid, D. Voulot, N. Warr, K. Wimmer, K. Wrzosek-Lipska, C. Y. Wu, and M. Zielinska, *Nature* **497**, 199 (2013).
- [16] P. A. Butler, L. P. Gaffney, P. Spagnoletti, K. Abrahams, M. Bowry, J. Cederkäll, G. de Angelis, H. De Witte, P. E. Garrett, A. Goldkuhle, C. Henrich, A. Illana, K. Johnston, D. T. Joss, J. M. Keatings, N. A. Kelly, M. Komorowska, J. Konki, T. Kröll, M. Lozano, B. S. Nara Singh, D. O'Donnell, J. Ojala, R. D. Page, L. G. Pedersen, C. Raison, P. Reiter, J. A. Rodriguez, D. Rosiak, S. Rothe, M. Scheck, M. Seidlitz, T. M. Shneidman, B. Siebeck, J. Sinclair, J. F. Smith, M. Stryczyk, P. Van Duppen, S. Vinals, V. Virtanen, N. Warr, K. Wrzosek-Lipska, and M. Zielinska, *Phys. Rev. Lett.* **124**, 042503 (2020).
- [17] R. F. Garcia Ruiz, R. Berger, J. Billowes, C. L. Binnertley, M. L. Bissell, A. A. Breier, A. J. Brinson, K. Chrysalidis, T. E. Cocolios, B. S. Cooper, K. T. Flanagan, T. F. Giesen, R. P. de Groote, S. Franchoo, F. P. Gustafsson, T. A. Isaev, Á. Koszorús, G. Neyens, H. A. Perrett, C. M. Ricketts, S. Rothe, L. Schweikhard, A. R. Vernon, K. D. A. Wendt, F. Wienholtz, S. G. Wilkins, and X. F. Yang, *Nature* **581**, 396 (2020).
- [18] S. M. Udrescu, S. G. Wilkins, A. A. Breier, R. F. G. Ruiz, M. Athanasakis-Kaklamanakis, M. Au, I. Belošević, R. Berger, M. L. Bissell, K. Chrysalidis, T. E. Cocolios, R. P. de Groote, A. Dorne, K. T. Flanagan, S. Franchoo, K. Gaul, S. Geldhof, T. F. Giesen, D. Hanstorp, R. Heinke, Á. Koszorús, S. Kujanp, L. Lalanne, G. Neyens, M. Nichols, H. A. Perrett, J. R. Reilly, S. Rothe, B. van den Borne, Q. Wang, J. Wessolek, X. F. Yang, and C. Zülch, *Nat. Phys.* **20**, 202 (2024), <https://doi.org/10.1038/s41567-023-02296-w>.
- [19] M. Athanasakis-Kaklamanakis, S. G. Wilkins, L. V. Skripnikov, A. Koszorus, A. A. Breier, M. Au, I. Belošević, R. Berger, M. L. Bissell, A. Borschevsky, A. Brinson, K. Chrysalidis, T. E. Cocolios, R. P. de Groote, A. Dorne, C. M. Fajardo-Zambrano, R. W. Field, K. T. Flanagan, S. Franchoo, R. F. G. Ruiz, K. Gaul, S. Geldhof, T. F. Giesen, D. Hanstorp, R. Heinke, T. A. Isaev, A. A. Kyuberis, S. Kujanpaa, L. Lalanne, G. Neyens, M. Nichols, L. F. Pasteka, H. A. Perrett, J. R. Reilly, S. Rothe, S. M. Udrescu, B. van den Borne, Q. Wang, J. Wessolek, X. F. Yang, and C. Zülch, arXiv:2308.14862 <https://doi.org/10.48550/arXiv.2308.14862> (2023).
- [20] P. J. Mohr, *Annals of Physics* **88**, 26 (1974).
- [21] S. A. Blundell, *Phys. Rev. A* **47**, 1790 (1993).
- [22] S. M. Schneider, W. Greiner, and G. Soff, *Phys. Rev. A* **50**, 118 (1994).
- [23] P. J. Mohr, G. Plunien, and G. Soff, *Phys. Rep.* **293**, 227 (1998).
- [24] P. Sunnergren, H. Persson, S. Salomonson, S. M. Schneider, I. Lindgren, and G. Soff, *Phys. Rev. A* **58**, 1055 (1998).
- [25] L. Labzowsky, I. Goidenko, M. Tokman, and P. Pyykkö, *Phys. Rev. A* **59**, 2707 (1999).
- [26] A. N. Artemyev, V. M. Shabaev, V. A. Yerokhin, G. Plunien, and G. Soff, *Phys. Rev. A* **71**, 062104 (2005).

- [27] S. G. Karshenboim, *Physics Reports* **422**, 1 (2005).
- [28] P. Indelicato, J. P. Santos, S. Boucard, and J.-P. Desclaux, *Eur. Phys. J. D* **45**, 155 (2007).
- [29] C. Thierfelder and P. Schwerdtfeger, *Phys. Rev. A* **82**, 062503 (2010).
- [30] V. M. Shabaev, I. I. Tupitsyn, and V. A. Yerokhin, *Phys. Rev. A* **88**, 012513 (2013).
- [31] P. Schwerdtfeger, L. F. Pašteka, A. Punnett, and P. O. Bowman, *Nuclear Physics A* **944**, 551 (2015), special Issue on Superheavy Elements.
- [32] J. S. M. Ginges and J. C. Berengut, *Journal of Physics B: Atomic, Molecular and Optical Physics* **49**, 095001 (2016).
- [33] J. S. M. Ginges and J. C. Berengut, *Phys. Rev. A* **93**, 052509 (2016).
- [34] O. Smits, P. Indelicato, W. Nazarewicz, M. Piibeleht, and P. Schwerdtfeger, *Physics Reports* **1035**, 1 (2023), pushing the limits of the periodic table — A review on atomic relativistic electronic structure theory and calculations for the superheavy elements.
- [35] K. Koziol, C. A. Giménez, and G. A. Aucar, *J. Chem. Phys.* **148**, 044113 (2018).
- [36] A. Sunaga and T. Saue, *Molecular Physics* **119**, e1974592 (2021).
- [37] L. V. Skripnikov, D. V. Chubukov, and V. M. Shakhova, *J. Chem. Phys.* **155**, 144103 (2021), https://pubs.aip.org/aip/jcp/article-pdf/doi/10.1063/5.0068267/13305693/144103_1.online.pdf.
- [38] A. Sunaga, M. Salman, and T. Saue, *J. Chem. Phys.* **157**, 164101 (2022), https://pubs.aip.org/aip/jcp/article-pdf/doi/10.1063/5.0116140/16552014/164101_1.online.pdf.
- [39] A. Zaitsevskii, L. V. Skripnikov, N. S. Mosyagin, T. Isaev, R. Berger, A. A. Breier, and T. Giesen, *J. Chem. Phys.* **in press** (2022).
- [40] M. T. Colombo Jofré, K. Koziol, I. A. Aucar, K. Gaul, R. Berger, and G. A. Aucar, *J. Chem. Phys.* **157**, 064103 (2022).
- [41] D. J. Flynn, I. P. Grant, and H. M. Quniey, *ArXiv e-prints* (2024), arXiv:2405.11262v2 [physics.atom-ph].
- [42] D. J. Flynn, I. P. Grant, and H. M. Quniey, *ArXiv e-prints* (2024), arXiv:2405.11261v2 [physics.atom-ph].
- [43] L. F. Pašteka, E. Eliav, A. Borschevsky, U. Kaldor, and P. Schwerdtfeger, *Phys. Rev. Lett.* **118**, 023002 (2017).
- [44] E. A. Uehling, *Phys. Rev.* **48**, 55 (1935).
- [45] A. M. Frolov and D. M. Wardlaw, *The European Physical Journal B* **85**, 348 (2012).
- [46] L. W. Fullerton and G. A. Rinker, *Phys. Rev. A* **13**, 1283 (1976).
- [47] E. H. Wichmann and N. M. Kroll, *Phys. Rev.* **101**, 843 (1956).
- [48] G. Källen and A. Sabry, *Mat. Fys. Medd. K. Dan. Vidensk. Selsk.* **29**, 17 (1955).
- [49] V. V. Flambaum and J. S. M. Ginges, *Phys. Rev. A* **72**, 052115 (2005).
- [50] P. Pyykkö and L.-B. Zhao, *Journal of Physics B: Atomic, Molecular and Optical Physics* **36**, 1469 (2003).
- [51] T. Beier, P. J. Mohr, H. Persson, and G. Soff, *Phys. Rev. A* **58**, 954 (1998).
- [52] P. Indelicato and P. J. Mohr, *Phys. Rev. A* **58**, 165 (1998).
- [53] V. A. Yerokhin and V. M. Shabaev, *Phys. Rev. A* **64**, 012506 (2001).
- [54] S. Boucard and P. Indelicato, *Eur. Phys. J. D* **8**, 59 (2000).
- [55] V. Berestetskii, L. Pitaevskii, and E. Lifshitz, *Relativistic Quantum Theory* (Pergamon Press, Oxford, 1982).
- [56] P. J. Mohr and Y.-K. Kim, *Phys. Rev. A* **45**, 2727 (1992).
- [57] P. J. Mohr, *Phys. Rev. A* **46**, 4421 (1992).
- [58] P. J. Mohr, *Annals of Physics* **88**, 52 (1974).
- [59] S. A. Brück, N. Sahu, K. Gaul, and R. Berger, *J. Chem. Phys.* **158**, 194109 (2023).
- [60] K. Gaul and R. Berger, *J. Chem. Phys.* **152**, 044101 (2020), arXiv:1907.10432 [physics.chem-ph].
- [61] C. van Wüllen, *J. Chem. Phys.* **109**, 392 (1998).
- [62] W. R. Inc., *Mathematica*, Version 11.0, Champaign, IL, 2022.
- [63] R. Berger, N. Langermann, and C. van Wüllen, *Phys. Rev. A* **71**, 042105 (2005).
- [64] S. Nahrwold and R. Berger, *J. Chem. Phys.* **130**, 214101 (2009).
- [65] T. A. Isaev and R. Berger, *Phys. Rev. A* **86**, 062515 (2012).
- [66] C. Zülch, K. Gaul, S. M. Giesen, R. F. G. Ruiz, and R. Berger, arXiv **physics.chem-ph**, 2203.10333 (2022).
- [67] C. van Wüllen, *Z. Phys. Chem* **224**, 413 (2010).
- [68] R. Ahlrichs, M. Bär, M. Häser, H. Horn, and C. Kölmel, *Chem. Phys. Lett.* **162**, 165 (1989).
- [69] C. Chang, M. Pelissier, and P. Durand, *Physica Scripta* **34**, 394 (1986).
- [70] E. v. Lenthe, E. J. Baerends, and J. G. Snijders, *J. Chem. Phys.* **99**, 4597 (1993), https://pubs.aip.org/aip/jcp/article-pdf/99/6/4597/14776295/4597_1.online.pdf.
- [71] E. van Lenthe, E. J. Baerends, and J. G. Snijders, *J. Chem. Phys.* **101**, 9783 (1994), https://pubs.aip.org/aip/jcp/article-pdf/101/11/9783/9435003/9783_1.online.pdf.
- [72] E. van Lenthe, R. van Leeuwen, E. J. Baerends, and J. G. Snijders, *International Journal of Quantum Chemistry* **57**, 281 (1996).
- [73] W. Liu, C. van Wüllen, F. Wang, and L. Li, *J. Chem. Phys.* **116**, 3626 (2002).
- [74] L. Visscher and K. G. Dyall, *At. Data Nucl. Data Tables* **67**, 207 (1997).
- [75] P. A. M. Dirac, *Proc. Roy. Soc. Lond. A* **123**, 714 (1929).
- [76] J. C. Slater, *Phys. Rev.* **81**, 385 (1951).
- [77] S. H. Vosko, L. Wilk, and M. Nuisar, *Can. J. Phys.* **58**, 1200 (1980).
- [78] A. D. Becke, *Phys. Rev. A* **38**, 3098 (1988).
- [79] C. Lee, W. Yang, and R. G. Parr, *Phys. Rev. B* **37**, 785 (1988).
- [80] A. D. Becke, *J. Chem. Phys.* **98**, 1372 (1993).
- [81] K. Koziol and G. A. Aucar, *J. Chem. Phys.* **148**, 134101 (2018), https://pubs.aip.org/aip/jcp/article-pdf/doi/10.1063/1.5026193/15539369/134101_1.online.pdf.
- [82] S. G. Wilkins, H. A. Perrett, S. M. Udrescu, A. A. Kyuberis, L. F. Pašteka, M. Au, I. Belošević, R. Berger, C. L. Binnersley, M. L. Bissell, A. Borschevsky, A. A. Breier, A. J. Brinson, K. Chrysalidis, T. E. Cocolios, B. S. Cooper, R. P. de Groote, A. Dorne, E. Eliav, R. W. Field, K. T. Flanagan, S. Franchoo, R. F. G. Ruiz, K. Gaul, S. Geldhof, T. F. Giesen, F. P. Gustafsson, D. Hanstorp, R. Heinke, Á. Koszorús, S. Kujanpää, L. Lalanne, G. Neyens, M. Nichols, J. R. Reilly, C. M. Ricketts, S. Rothe, A. Sunaga, B. van den Borne, A. R. Vernon, Q. Wang, J. Wessolek, F. Wienholtz, X. F. Yang, Y. Zhou, and C. Zülch, *Ionization potential of radium monofluoride* (2024), arXiv:2408.14673

[physics.atom-ph].

[83] L. V. Skripnikov, *J. Chem. Phys.* **154**, 201101 (2021), https://pubs.aip.org/aip/jcp/article-pdf/doi/10.1063/5.0053659/14003441/201101_1_online.pdf.